Active Efficient Coding Explains the Development of Binocular Vision and its Failure in Amblyopia

Samuel Eckmann[a,1], **Lukas Klimmasch**[a], **Bertram Shi**[b], **and Jochen Triesch**[a]

[a]Frankfurt Institute for Advanced Studies FIAS, Frankfurt am Main, Germany; [b]Dept. of Electronic and Computer Engineering, HK University of Science and Technology, Clear Water Bay, Hong Kong

This manuscript was compiled on March 8, 2019

The development of vision during the first months of life is an active process that comprises the learning of appropriate neural representations and the learning of accurate eye movements. While it has long been suspected that the two learning processes are coupled, there is still no widely accepted theoretical framework describing this joint development. Here we propose a computational model of the development of active binocular vision to fill this gap. The model is based on a new formulation of the *Active Efficient Coding* theory, which proposes that eye movements, as well as stimulus encoding, are jointly adapted to maximize the overall coding efficiency of the system. Under healthy conditions, the model self-calibrates to perform accurate vergence and accommodation eye movements. It exploits disparity cues to deduce the direction of defocus, which leads to coordinated vergence and accommodation responses. In a simulated anisometropic case, where the refraction power of the two eyes differs, an amblyopia-like state develops, in which the foveal region of one eye is suppressed due to inputs from the other eye. After correcting for refraction errors, the model can only reach healthy performance levels if receptive fields are still plastic, in line with findings on a critical period for binocular vision development. Overall, our model offers a unifying conceptual framework for understanding the development of binocular vision under healthy conditions and in amblyopia.

efficient coding | active perception | amblyopia | vergence | accommodation

Despite making up only 2% of our body mass (1), our brains are responsible for 20% of our energy consumption (2). Therefore, organizing neural circuits to be energy efficient may provide a substantial evolutionary advantage. One means of increasing energy efficiency in sensory systems is to attune neural representations to the statistics of sensory signals. Based on this *Efficient Coding Hypothesis* (3), numerous experimental observations in different sensory modalities have been explained (4, 5). For instance, it has been shown that receptive field properties in the early visual pathway can be explained through models that learn to efficiently encode natural images (6, 7). These findings have extended classic results showing that receptive field shapes in visual cortex are highly malleable and a product of the organism's sensory experience (8–11).

Importantly, however, animals can shape the statistics of the sensory inputs through their behavior. This gives them additional degrees of freedom to optimize coding efficiency by jointly adapting their neural representations and behavior. This idea has recently been advanced as *Active Efficient Coding* (12, 13). It can be understood as a generalization of the efficient coding hypothesis to active perception (Fig. 1). Along these lines, *Active Efficient Coding* models have been able to explain the development of visual receptive fields and the self-calibration of smooth-pursuit and vergence eye movements (12, 13) as well as the development of the optokinetic nystagmus (14). This has been achieved by combining a sparse coding model, which learns to efficiently represent the sensory input, with simultaneous learning of, e.g., vergence or pursuit movements so as to minimize the encoding error of the sparse coding model.

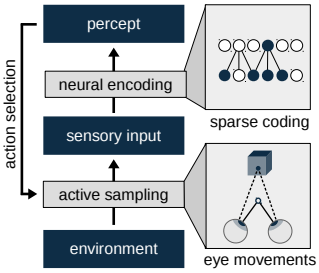

Fig. 1. The action-perception loop. The sensory input is obtained by actively sampling signals from the environment, e.g., via eye movements. A percept is formed by neural encoding. For example, in the early visual pathway this can be described by sparse coding (7). Finally, the current percept drives the selection of actions thereby shaping the sampling process.

A critical restriction of these previous models is that they assume an approximately constant amount of sensory information reaching each eye at any time. This assumption is invalid if, e.g., the control of accommodation is considered. For instance, if the eyes do not properly focus on the stimulus, high spatial frequencies will be lacking from the retinal images, reducing their information content.

Here we consider a novel and more general formulation of the *Active Efficient Coding* theory that solves this problem. We formalize the goal of maximizing coding efficiency as maximizing the mutual information $I(R;C)$ between the raw sensory input R and the cortical encoding C under a limited

Significance Statement

Brains must operate in an energy efficient manner. The efficient coding hypothesis states that sensory systems achieve this by adapting neural representations to the statistics of sensory input signals. Importantly, however, these statistics are influenced by the organism's behavior and how it samples information from the environment. Therefore, optimal performance requires jointly optimizing neural representations and behavior, a theory called *Active Efficient Coding*. Here we test the plausibility of this theory by proposing a computational model of the development of binocular vision. The model explains the development of accurate binocular vision under healthy conditions. In the case of refractive errors, however, the model develops an amblyopia-like state and predicts conditions for successful treatment.

SE, BS and JT designed the study. SE performed the simulations and analyzed the results. LK helped to implement the suppression model. SE and JT wrote the first draft of the paper.

The authors declare no conflict of interest.

[1]To whom correspondence should be addressed: eckmann@fias.uni-frankfurt.de

resource constraint. We decompose $I(R;C)$ as:

$$I(R;C) = \mathcal{H}(R) - \mathcal{H}(R|C) \ , \qquad [1]$$

where $H(R)$ is the (non-negative) Shannon entropy of the raw sensory response and $H(R|C)$ is the (non-negative) conditional entropy of the sensory input given the cortical encoding. Maximization of $I(R;C)$ can, therefore, be achieved by maximizing $H(R)$ and minimizing $H(R|C)$ at the same time. We demonstrate this approach through a concrete model of the development of binocular vision including the simultaneous calibration of vergence and accommodation control.

The *Active Efficient Coding* model we propose has a modular structure. A sparse coding model learns the cortical encoding C given the raw sensory input of two retinas R, while an accommodation controller learns to maximize $H(R)$ and a vergence controller learns to minimize $H(R|C)$. The three modules learn simultaneously and explain the development and calibration of high fidelity control of vergence and accommodation.

Newborns have difficulties bringing objects into focus and cannot yet verge their eyes properly (15). Only after several months of interacting with their visual environment, they achieve accurate control of vergence and accommodation. How infants manage to self-calibrate their control mechanisms is currently unknown. Further, in certain medical conditions the calibration of vergence and accommodation control is hindered. For example, anisometropia describes a condition of interocular differences in the refraction power of the two lenses. If not corrected early during development, this can evoke amblyopia: a disorder of the developing visual system that is characterized by an interocular difference in visual acuity that is not immediately resolved by refractive correction. Amblyopia can lead to a loss of stereopsis and in severe cases to monocular blindness (16). However, in anisometropic amblyopia stereopsis is maintained in the periphery and at low-spatial frequencies (17–19). Furthermore, vergence and accommodation eye movements are either less accurate or completely absent (20, 21).

Although there have been recent advances in the treatment of amblyopia (22, 23), existing treatment methods do not lead to satisfactory outcomes in all patients. This is aggravated by the fact that treatment success strongly depends on the stage of neuronal circuit maturation (22). When young patients are still in a critical period of circuit plasticity (11), they often recover after refraction errors are corrected, while adults mostly remain impeded (24, 25).

Below we show that the above findings are all readily explained by our model. Under healthy conditions, the model develops accurate vergence and accommodation eye movements. To find the direction of defocus the accommodation controller learns to recruit disparity information, which leads to coupled vergence and accommodation movements. In order to probe the plausibility of the model, we also test it under conditions of abnormal input. When the system is impaired due to monocular hyperopia, we observe that one eye suppresses the other and an amblyopia-like state develops. We show that this is due to the abnormal development of binocular receptive fields in the model and demonstrate how healthy binocular vision is regained when the sparse coding module readapts after refraction correction. However, if the sensory encoding is no longer plastic and does not adapt to the changes

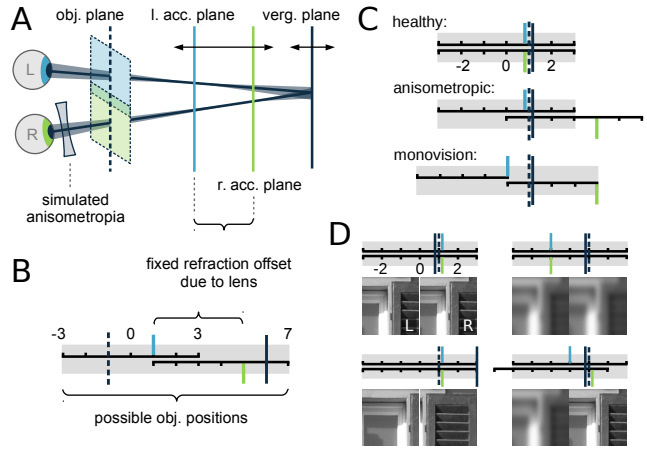

Fig. 2. Retinal input sampling from the environment. *(A)* Object position, eye focus, and eye fixation at different distances are represented as different plane positions. *(B)* Abstraction of *A*. The gray horizontal bar indicates the range where objects are presented during the simulation and also indicates the fixation range, i.e., possible vergence plane positions. Horizontal axes indicate reachable accommodation plane positions for the left (light blue) and right (green) eye. Note that when the stimulus is placed at, e.g., position 0 it cannot be focused by the right eye in this example. *(C)* Position range of accommodation and vergence planes under different conditions. Same scheme as in *B*. *(D)* Examples of retinal input images for different plane position configurations. For better visibility, disparity shifts and blur are increased compared to actual values.

in the visual input statistics, suppression prevails. Finally, when hyperopia is induced in one eye and myopia in the other, monovision develops, i.e., distant stimuli are focused with the hyperopic eye and close stimuli with the myopic eye. This is in line with observations of human patients (26).

Model Formulation. Our model comprises an observer looking at a textured planar object. The object is sampled by the two eyes for ten subsequent iterations which constitute one fixation. After each fixation, a new object is presented at a new, random distance. The sensory input can be manipulated by accommodation and vergence eye movements (Fig. 2). The resulting retinal images are whitened monocularly and then binocularly encoded by a population of cortical neurons. In our model, the cortical population activity represents the binocular 'percept' from which behavioral commands are generated (compare Fig. 1, top).

At the cortical stage, we use two binocular sparse coders to efficiently encode the binocular retinal images with a weighted set of bases (see Methods): One for fine details in the foveal region and one for the periphery that receives a low-pass filtered input. All bases are adjusted online to reflect the stimulus statistics, e.g., via their disparity and frequency tuning distributions (27) and resemble receptive fields of simple cells in the visual cortex (7) (Fig. 3, center).

We further employ a basic interocular suppression model (Fig. 4) to describe dynamic contrast modulation based on the ocular balance of the input encoding. If mostly right (left) monocular bases are recruited by the sparse coder, the contrast of the right(left) eye input is enhanced in subsequent iterations. This is in agreement with reciprocal excitation of similarly tuned neurons in visual cortex (28, 29). At the same time, the total input energy is kept constant to ensure similar activity levels for monocular and binocular visual experience as observed experimentally at high contrast levels (30) (see

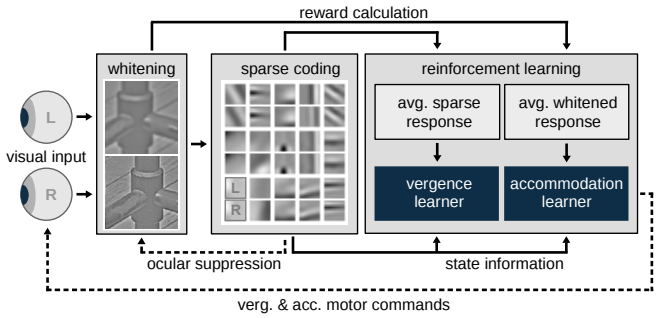

Fig. 3. Model architecture with solid arrows representing the flow of sensory information and dashed arrows representing the flow of control commands. Only one scale is shown. Sampled input images with given blur and disparity are whitened (left). Thereafter, they are sparsely encoded by a set of binocular bases in analogy to V1 simple cells. In the healthy case, without refraction errors, receptive fields are mostly binocular and tuned towards zero disparity (center). The population-averaged sparse activity serves as state information for two reinforcement learners (right) which control vergence and accommodation commands, respectively. Accommodation commands are learned to maximize the mean squared response after whitening (avg. whitened response). The reward for the vergence learner is the negative reconstruction error of the sparse encoding stage which can be read out as the average squared sparse response (see Methods).

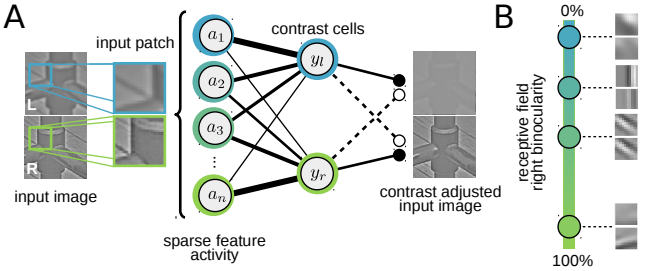

Fig. 4. Interocular suppression model. *(A)* When mostly right(left) monocular feature bases a_j are used to encode an input patch, the right(left) contrast cell $y_r(y_l)$ becomes activated and the left(right) retinal image is suppressed. Dashed(solid) lines indicate inhibitory(excitatory) interactions. Connection strength is represented by line thickness. We model interocular suppression to be scale specific, i.e., when the foveal region of the left eye is suppressed, the periphery of the left eye may still provide unattenuated input (see Methods for details). *(B)* Binocularity of five bases; from mostly right monocular (blue) to almost exclusively left monocular (green).

Methods).

In our model, not only stimulus encoding but also stimulus selection, i.e., behavior, is optimized to maximize coding efficiency. We define maximizing coding efficiency as maximizing the mutual information I between the retinal response R and the cortical represenation C [1] under the limited resource constraint of a constant number of active neurons (compare Fig. 1 and Fig. 3). Maximizing the entropy of the retinal input $H(R)$ lets the system favor inputs with high spatial frequencies. This is due to the edge-enhancing nature of retinal ganglion cell receptive fields. With their center-surround receptive fields, they are selective for sharp constrasts and respond poorly when out of focus input is presented. Their receptive field shape has also been interpreted as a result of maximizing coding efficiency (6, 31). We assume the spatial frequency tuning of retinal ganglion cells to be static and thus independent of the distribution of spatial frequencies in the retinal input as suggested by deprivation experiments (10, 32, 33).

The second term in [1] is the negative conditional entropy of the retinal representation given the cortical representation. This term can be understood as the information that is lost, i.e., not encoded, at the cortical stage. By minimizing lost information a second reinforcement learner that controls vergence behavior (Fig. 3) favors stimuli with highly correlated left and right eye inputs. Both terms in [1] can be approximated with the average population activity at the cortical and retinal stage, respectively (Fig. 3) (see Methods). Thus, vergence and accommodation controllers jointly maximize sensory coding efficiency.

Results

Active Efficient Coding Leads to Self-calibration of Active Binocular Vision. Images were positioned in front of the observer at random distances. After ten iterations, i.e., one fixation, the image is replaced with a new image at a new random distance (see Methods for details). The agent controls its retinal input by shifting accommodation and vergence planes along the egocentric axis (Fig. 2). Dependent on the binocularity of the activated bases the contrast of the respective eye is suppressed (Fig. 4). In the healthy condition without refraction errrors and coinciding left and right accommodation planes (Fig. 2C, top), the model learns to perform precise vergence eye movements (Fig. 5A and B) while most neurons develop binocular receptive fields (Fig. 3, center and Fig. 7B).

Accommodation performance is highly accurate as well. This is achieved without obvious sign cues: defocus blur changes linearly independent of whether an eye focuses behind or in front of the object (SI Appendix, Fig. S1). Also, neither chromatic (34) nor other higher order aberrations (35) are provided in our model, which could help to steer focus in the right direction. We found that instead, input disparity is utilised to shift focus in the correct direction (SI Appendix, Fig. S3, bottom row). The system capitalizes on the unison movement of the vergence and accommodation planes such that the sign of defocus is inferred from disparity cues (SI Appendix, Fig. S3).

Model correctly describes response to unnatural visual input. The impact of input disparity on the accommodation policy becomes even more apparent when 'unnatural' input is presented. We placed virtual prisms in front of the eyes, which change the vergence target distance while the accommodation target distance remains unaltered (Fig. 6A). In response, accommodation focus erroneously shifts in the direction of the new fixation target plane. When we remove the prisms one observes the same effect in the opposite direction. This behavior is in accordance with experiments (36) and can lead to visual fatigue and discomfort while using virtual reality head-mounted displays (37).

We also examined the short-term effect of lens-induced anisometropia on a model trained under healthy conditions. By introducing a refraction error to one eye, the left and the right accommodation plane are now separated such that only one of the retinal images can be in focus at any given time (Fig. 2C, center). As was previously suggested (38), when we present a stimulus moving in small steps the system chooses to continuously focus with one or the other eye dependent on the initial stimulus position (SI Appendix, Fig. S4). However, when objects are positioned at random distances both eyes are alternately prioritized to focus the object (Fig. 6B). In accordance with experimental data (38), vergence performance was slightly decreased compared to the healthy case.

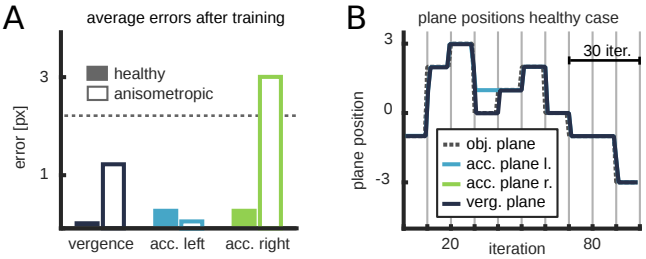

Fig. 5. Model performance under healthy and anisometropic conditions. *(A)* Average absolute vergence and accommodation errors after training under healthy and anisometropic conditions. Dashed line indicates the average error for random plane movements in healthy case. *(B)* Example trajectories of plane positions (pos.) after training for the healthy case. Vertical gray lines indicate end of fixation where stimulus distance and image are randomly switched. Most of the time, all plane positions coincide.

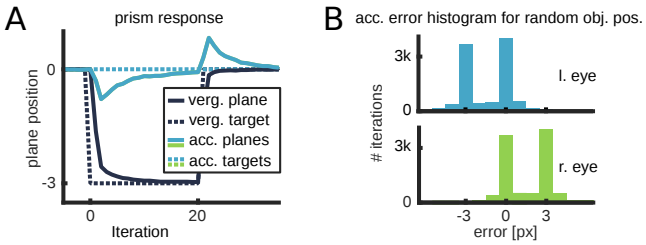

Fig. 6. Vergence-accommodation coupling after training under healthy conditions. *(A)* Average vergence and accommodation plane trajectories while adding and removing additional lenses at iteration 0 and 20, respectively. Target planes which yield zero disparity (dark blue) and zero blur (light blue) are shown as dotted lines. *(B)* Accommodation error histogram after training under anisometropic conditions for random object positions.

Anisometropia drives model into amblyopic state. To test how the model evolves under abnormal rearing conditions, we simulated an anisometropic case by adding a simulated lens in front of the right eye such that it became hyperopic and was unable to focus objects at close distances (Fig. 2*C*, center). Different from the healthy case where none of the eyes is favored over the other, in the anisometropic case an amblyopia-like state emerges. Foveal input from the hyperopic eye is suppressed (SI Appendix, Fig. S2*C*) while the peripheral input is unaffected and still provides binocular information such that a coarse control of vergence is maintained (Fig. 5*A* and SI Appendix, Fig. S2*B*). This results in stable binocular receptive fields in the periphery which may provide enough information for coarse stereopsis as observed in experiments (17–19). Accommodation adapts such that the stimulus is continuously tracked with the unimpaired eye (SI Appendix, Fig. S5).

Early but not late diffraction correction rescues binocular vision. To test if the anisopmetropic model can recover from amblyopia upon correction of the refraction error, we first trained a fully plastic system under anisometropic conditions until it reached stable performance. Then, all refraction errors were corrected. When the receptive fields were fixed upon refraction error correction, receptive fields remained monocular and the system did not recover. Instead, it maintained a high level of vergence error (Fig. 7*A*, dotted line). In contrast, when bases remained plastic and could adapt to the changed input statistics suppression of the formerly impaired eye was lifted (Fig. 7*A* and SI Appendix, Fig. S6), solid lines). This was due to a shift from monocular to binocular receptive fields as a result of the changed input statistics (Fig. 7*B*). This is in line with a large body of evidence suggesting that limited cortical plasticity prevents recovery from amblyopia after the correction of refractive errors (11, 22, 23).

Unbiased Anisometropia Evokes Monovision. We wondered if anisometropic suppression would also develop if both eyes were similarly impaired but with opposite sign of the refractive error. We adjusted the parameters such that the left eye was myopic and the right eye hyperopic. Objects were placed between the minimum focusable position of the myopic eye and the maximum focusable distance of the hyperopic eye (Fig. 2*C*, bottom). This configuration is similar to monovision, a treatment method for presbyopia where the ametropic condition is achieved via optical lenses or surgery (26). In such cases, the myopic eye is used for near and the hyperopic eye for distant vision. Thereby, the required amount of accommodation is reduced. In our model we observe the same effect (SI Appendix, Fig. S7*A* and *C*). None of the two eyes is supprssed permanently, although foveal receptive fields are mostly monocular. Rather, when distant objects are focused the myopic eye is suppressed and when close stimuli are presented the hyperopic eye is suppressed. When either one of the eyes could be utilized to focus on a stimulus hysteresis develops, i.e., when the left eye was suppressed in the previous fixation the right eye is used to focus and vice versa (SI Appendix, Fig. S7*B*).

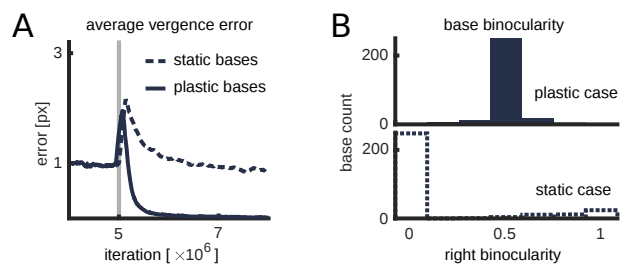

Fig. 7. Model performance after treatment. *(A)* Vergence performance of formerly anisometropic systems after correction of all refraction errors at iteration 5×10^6 (vertical gray line). The (dotted)solid line indicates system with (non-)plastic receptive fields. *(C)* Histogram of foveal receptive field binocularity $b_{(\cdot,r)}$ after refraction error correction (see Methods for details).

Discussion

We have shown how optimizing both behavior and encoding for efficiency leads to the self-calibration of active binocular vision. Specifically, our model, which is based on a new formulation of the *Active Efficient Coding* theory, accounts for the simultaneous development of vergence and accommodation. Under healthy conditions, the model develops accurate vergence and accommodation eye movements. For a simulated anisometropia, however, where one eye suffers from a refraction error while the other eye is unaffected, it develops into an amblyopia-like state with monocular receptive fields and loss of stereopsis. Recovery from this amblypia-like state is only possible if receptive fields in the model remain plastic, matching findings on a critical period for binocular development. Furthermore, when both eyes have opposite refraction errors, a form of monovision develops, where the myopic eye is used to focus near objects and the hyperopic eye is used for far objects. Thus, the model explains a range of findings from a unified computational perspective of coding efficiency.

While we have focused on the development of active binocular vision including accommodation and vergence control, our formulation of *Active Efficient Coding* is very general and could be applied to many active perception systems across species and sensory modalities. *Active Efficient Coding* is rooted in classic efficient coding ideas (3–7), of which predictive coding theories are special examples (39, 40). Classic efficient coding does not consider optimizing behavior, however. Friston's Active Inference approach does consider the generation of behavior in a very general fashion. There, motor commands are generated so as to fulfill certain sensory predicitons. In our new formulation of *Active Efficient Coding*, motor commands are learned to maximize the mutual information between the sensory input and its internal representation. This implies maximizing the amount of sensory information sampled from the environment and avoids the problem of deliberately using accommodation to defocus the eyes (or the agent closing the eyes altogether) to make the sensory input easy to encode and/or predict. As such, our approach is more related to Schmidhuber's ideas on maximizing compression progress (41).

Interestingly, when learning to accommodate the model discovers a way to exploit disparity cues for determining the direction of defocus. This leads to a coupling of vergence and accommodation as observed experimentally (42). Humans are believed to use additional sign cues for determining the direction of defocus (34, 35, 42). We deliberately excluded such cues from the model to emphasize the fact that they are not strictly necessary to learn accurate accommodation control under otherwise healthy conditions. Investigating how such additional cues might affect the accommodation performance of our model under impaired conditions is left for future work.

Other aspects of our model are also greatly simplified compared to biology. An important example is the inter-ocular suppression mechanism. The simple logic behind the used suppression mechanism is that every "neuron" tries to maximize its own activity by suppressing competing input from the other eye. This proved sufficient to account for the development of an amblyopia-like state, with the development of mostly monocular receptive fields in the representation of the fovea. More sophisticated suppression models could be incorporated in the future (46), but we do not expect them to change the conclusions from the present model. However, a topic of current interest is how suppression develops during disease development and also during treatment, e.g., with the standard patching method. A better understanding of the role of suppression in amblyopia could lead to improved therapies in the future.

Interestingly, accommodation performance also deteriorates under pathological conditions such as down syndrome (43) or autism (44) relative to healthy subjects (42). How these changes relate to the underlying neural circuits, however, is poorly understood (45). Our model may provide a useful starting point for theorizing about deficits in accommodation control in different disorders.

Materials and Methods

Retinal Image Rendering. We used 300 natural images of the man-made category from the McGill Calibrated Colour Image Database (47) and converted them to grayscale. Images were presented at random positions (see Fig. 2*A* and *B*) for one fixation, i.e., 10 subsequent iterations, before the next image was randomly selected. The foveal images of the left and the right eye (110×110 pixels each) were sampled from the center of the original image and normalized to zero mean and unit variance. For every 1 a.u. distance between vergence and object plane the left/right foveal window was shifted 1px to the left/right. A Gaussian blur filter was applied to the left and the right foveal image were the standard deviations depend linearly on the distance between accommodation and vergence planes. 1 a.u. distance corresponds to 0.8px of standard deviation (SI Appendix, Fig. S2C).

Input processing. The left and right foveal image were whitened as described by Olshausen and Field (7), independent of accommodation or vergence. Images were cut and merged into 121 binocular patches of size 16×8 px. Image patches were normalized to zero mean and unit variance and subsequently sparsely encoded with the matching pursuit algorithm (48), where we recruited $n = 10$ out of 300 bases ϕ_i from the dictionary in order to reduce the reconstruction error $|\Phi_n|^2$, i.e., the energy of the residual after n iterations.

$$\Phi_n = \Phi_0 - \Phi_n^{(s)} \equiv \Phi_0 - \sum_{k=1}^{n} \alpha_{i_k} \phi_{i_k},$$

$$\alpha_{i_j} = \langle \phi_{i_j}, \Phi_{j-1} \rangle, \quad i_k = \underset{j}{\operatorname{argmax}} \left(\langle \phi_j, \Phi_{k-1} \rangle \right).$$

Here, Φ_0 is the normalized input patch. $\Phi_n^{(s)}$ is the sparsely encoded image patch and α_{i_k} the respective base activities. For a second, peripheral scale the input images were downsampled with a Gaussian pyramid by a factor of 2. Again, two 110×110 px windows were extracted and merged into 121 binocular patches. They were encoded by a second sparse coder with its own filter bank.

Reinforcement Learning. We used two separate natural actor critic reinforcement learners (RLs) (49) as presented in (13) to control the accommodation planes and the vergence plane, respectively. The plane positions can be changed in steps of [-2, -1, 0, 1, or 2] (compare Fig. 2). The state information for both RLs are the patch-averaged squared responses of the foveal and the peripheral scale bases of both matching pursuit dictionaries. The reward for the vergence learner is the negative reconstruction error of the matching pursuit algorithm, i.e., the average squared response of the base activity after patch encoding averaged over pixel values, patches, and scales. The reward for the accommodation learner is the average absolute squared pixel value of the whitened binocular image. Both rewards were normalized online to zero mean and unit variance.

Maximizing Mutual Information. Rewards for the reinforcement learners are the average response after whitening and encoding, respectively. Together these can be understood as a proxy for the mutual information between the whitened Φ_0 and sparse response $\Phi_n^{(s)}$:

$$I(\Phi_0, \Phi_n^{(s)}) = H(\Phi_0) - H(\Phi_0 | \Phi_n^{(s)}),$$

where we take each response value as a sample of a random variable and further assume that the conditional entropy $H(\Phi_0|\Phi_n^{(s)})$, can be understood as a reconstruction error, i.e., all information in the retinal image that is not encoded at the cortical stage. In terms of the sparse coding algorithm, this corresponds to the energy of residual image $|\Phi_n|^2$ (7). Finally, we make use of the 'energy conservation' property of the matching pursuit (48) which holds if we can assume that the n dictionary elements recruited for encoding are pairwise orthogonal:

$$-|\Phi_n|^2 = -|\Phi_0|^2 + \sum_j |\alpha_j|^2.$$

Since the input energy $|\Phi_0|^2$ does not depend on vergence for isotropic input statistics and is normalized to unity, we take the energy of the sparse response as the reward for the vergence learner. For the accommodation learner we make the assumption of gaussian

distributed pixel values. Thus, we can maximize the energy of the respective responses instead of their full entropy:

$$H(\Phi_0) \to \ln\left(\sqrt{2\Pi e \sigma^2_{\Phi_0}}\right) \sim \sigma^2_{\Phi_0} = |\Phi_0|^2,$$

since $\ln(\sqrt{\sigma^2})$ is monotone in σ^2. Together, this leaves us with the energy of the whitened response for the accommodation and the energy of the sparse response for the vergence reward. This form has the advantage that it is straightforward to measure the average population activity in biological systems.

Suppression Mechanism. The suppression mechanism adjusts the contrast of left and right input image after whitening based on the binocularity of the previously encoded images (see Fig. 4). Every neuron tries to stabilize its own activity by (suppressing) enhancing (un)favorable stimuli. We calculate the binocularity index of neuron i as

$$b_{(i,c)} = \frac{||\phi_{(i,c)}||}{||\phi_{(i,c)}|| + ||\phi_{(i,\bar{c})}||}, \quad c \in \{l, r\},$$

where $\phi_{(i,c)}$ is the monocular receptive subfield of neuron i and $||\cdot||$ is the euclidean norm. The current activity of encoding neurons is weighted with their binocularity indices and subsequently passed through the non-linearity of a contrast neuron:

$$\tau \frac{\mathrm{d}x_c}{\mathrm{d}t} = -x_c + \sum_i a_i^{(t)} b_{(i,c)},$$
$$y_c^{(t)} = \frac{s}{1-\theta}[x_c^{(t)} - \theta]_+.$$

We choose the threshold $\theta = 0.6$ and the saturation $s = 0.8$. Finally, the input patches for the sparse coder are normalized to

$$\Phi_c^{(t+1)} \to \Phi_c^{(t+1)}\left(1 + y_c^{(t)} - y_{\bar{c}}^{(t)}\right).$$

Software and Documentation. Documented MATLAB® code of the model will be made available after publication

ACKNOWLEDGMENTS. This work was supported by the German Federal Ministry of Education and Research under Grants 01GQ1414 and 01EW1603A, the Hong Kong Research Grants Council under Grant 618713, and the Quandt Foundation. We thank Maria Fronius and Rowan Candy for numerous discussions.

1. Dekaban AS, Sadowsky D (1978) Changes in brain weights during the span of human life: relation of brain weights to body heights and body weights. *Annals of Neurology: Official Journal of the American Neurological Association and the Child Neurology Society* 4(4):345–356.
2. Clark DD, Sokoloff L (1999) Circulation and energy metabolism of the brain in *Basic Neurochemistry: Molecular, Cellular and Medical Aspects*, eds. Siegel GJ, Agranoff BW, Albers RW, Fisher SK, Uhler MD. (Lippincott-Raven, Philadelphia), p. 637–670.
3. Barlow HB (1961) Possible Principles Underlying the Transformations of Sensory Messages in *Sensory Communication*.
4. Simoncelli EP, Olshausen BA (2001) Natural image statistics and neural representation. *Annual review of neuroscience* 24(1):1193–1216.
5. Lewicki MS (2002) Efficient coding of natural sounds. *Nature neuroscience* 5(4):356.
6. Atick JJ, Redlich AN (1992) What does the retina know about natural scenes? *Neural computation* 4(2):196–210.
7. Olshausen BA, Field DJ (1997) Sparse coding with an overcomplete basis set: A strategy employed by v1? *Vision research* 37(23):3311–3325.
8. Wiesel TN, Hubel DH (1963) Single-cell responses in striate cortex of kittens deprived of vision in one eye. *Journal of neurophysiology* 26(6):1003–1017.
9. Hirsch HV, Spinelli D (1970) Visual experience modifies distribution of horizontally and vertically oriented receptive fields in cats. *Science* 168(3933):869–871.
10. Movshon JA, Van Sluyters RC (1981) Visual neural development. *Annual review of psychology* 32(1):477–522.
11. Espinosa JS, Stryker MP (2012) Development and Plasticity of the Primary Visual Cortex. *Neuron* 75(2):230–249.
12. Zhao Y, Rothkopf CA, Triesch J, Shi BE (2012) A unified model of the joint development of disparity selectivity and vergence control in *Development and Learning and Epigenetic Robotics (ICDL), 2012 IEEE International Conference on*. (IEEE), pp. 1–6.
13. Teulière C, et al. (2015) Self-calibrating smooth pursuit through active efficient coding. *Robotics and Autonomous Systems* 71:3–12.
14. Zhang C, Triesch J, Shi BE (2016) An active-efficient-coding model of optokinetic nystagmus. *Journal of vision* 16(14):10–10.
15. Tondel GM, Candy TR (2008) Accommodation and vergence latencies in human infants. *Vision research* 48(4):564–576.
16. Blakemore C, Van Sluyters RC (1974) Experimental analysis of amblyopia and strabismus. *The British journal of ophthalmology* 58(3):176.
17. Holopigian K, Blake R, Greenwald MJ (1986) Selective losses in binocular vision in anisometropic amblyopes. *Vision research* 26(4):621–630.
18. Bradley A, Freeman RD (1981) Contrast sensitivity in anisometropic amblyopia. *Investigative Ophthalmology and Visual Science* 21(3):467–476.
19. Babu RJ, Clavagnier S, Bobier WR, Thompson B, Hess RF (2017) Regional extent of peripheral suppression in amblyopia. *Investigative Ophthalmology and Visual Science* 58(4):2329–2340.
20. Kenyon RV, Ciuffreda K, Stark L (1980) Dynamic vergence eye movements in strabismus and amblyopia: symmetric vergence. *Investigative ophthalmology & visual science* 19(1):60–74.
21. Manh V, Chen AM, Tarczy-Hornoch K, Cotter SA, Candy TR (2015) Accommodative performance of children with unilateral amblyopia. *Investigative ophthalmology & visual science* 56(2):1193–1207.
22. Levi DM, Knill DC, Bavelier D (2015) Stereopsis and amblyopia: A mini-review.
23. Stryker MP, Loewel S (2018) Amblyopia: New molecular/pharmacological and environmental approaches. *Visual neuroscience* 35.
24. Cotter SA, Group PEDI, , et al. (2006) Treatment of anisometropic amblyopia in children with refractive correction. *Ophthalmology* 113(6):895–903.
25. Steele AL, et al. (2006) Successful treatment of anisometropic amblyopia with spectacles alone. *Journal of American Association for Pediatric Ophthalmology and Strabismus* 10(1):37–43.
26. Evans BJ (2007) Monovision: A review. *Ophthalmic and Physiological Optics* 27(5):417–439.
27. Hunt JJ, Dayan P, Goodhill GJ (2013) Sparse Coding Can Predict Primary Visual Cortex Receptive Field Changes Induced by Abnormal Visual Input. *PLoS Computational Biology* 9(5).
28. Yoshioka T, Blasdel GG, Levitt JB, Lund JS (1996) Relation between patterns of intrinsic lateral connectivity, ocular dominance, and cytochrome oxidase-reactive regions in macaque monkey striate cortex. *Cerebral Cortex* 6(2):297–310.
29. Iacaruso MF, Gasler IT, Hofer SB (2017) Synaptic organization of visual space in primary visual cortex. *Nature* 547(7664):449–452.
30. Moradi F, Heeger DJ (2009) Inter-ocular contrast normalization in human visual cortex. *Journal of Vision* 9(3):13–13.
31. Pitkow X, Meister M (2012) Decorrelation and efficient coding by retinal ganglion cells. *Nature neuroscience* 15(4):628.
32. Sherman SM, Stone J (1973) Physiological normality of the retina in visually deprived cats. *Brain Research* 60(1):224–230.
33. Movshon JA, et al. (1987) Effects of early unilateral blur on the macaque's visual system. iii. physiological observations. *Journal of Neuroscience* 7(5):1340–1351.
34. Zannoli M, Love GD, Narain R, Banks MS (2016) Blur and the perception of depth at occlusions. *Journal of Vision* 16(6):17–17.
35. Chen L, Kruger PB, Hofer H, Singer B, Williams DR (2006) Accommodation with higher-order monochromatic aberrations corrected with adaptive optics. *Journal of the Optical Society of America. A, Optics, image science, and vision* 23(1):1–8.
36. Bharadwaj SR, Candy TR (2009) Accommodative and vergence responses to conflicting blur and disparity stimuli during development. *Journal of vision* 9(11):4.1–18.
37. Hoffman DM, Girshick AR, Akeley K, Banks MS (2008) Vergence-accommodation conflicts hinder visual performance and cause visual fatigue. *Journal of vision* 8(3):33–33.
38. Bharadwaj SR, Rowan Candy T (2011) The effect of lens-induced anisometropia on accommodation and vergence during human visual development. *Investigative Ophthalmology and Visual Science*.
39. Ballard DH (1991) Animate vision. *Artificial Intelligence* 48(1):57–86.
40. Friston K (2010) The free-energy principle: a unified brain theory? *Nature reviews neuroscience* 11(2):127.
41. Schmidhuber J (2008) Driven by compression progress: A simple principle explains essential aspects of subjective beauty, novelty, surprise, interestingness, attention, curiosity, creativity, art, science, music, jokes in *Workshop on Anticipatory Behavior in Adaptive Learning Systems*. (Springer), pp. 48–76.
42. Bharadwaj SR, Candy TR (2008) Cues for the control of ocular accommodation and vergence during postnatal human development. *Journal of Vision* 8(16):14–14.
43. Doyle L, Saunders KJ, Little JA (2017) Determining the relative contribution of retinal disparity and blur cues to ocular accommodation in Down syndrome. *Scientific Reports* 7(July 2016):1–8.
44. Anketell PM, Saunders KJ, Gallagher SM, Bailey C, Little JA (2018) Accommodative Function in Individuals with Autism Spectrum Disorder. *Optometry and Vision Science* 95(3):193–201.
45. Robertson CE, Baron-Cohen S (2017) Sensory perception in autism. *Nature Reviews Neuroscience*.
46. Hess RF, Thompson B (2015) Amblyopia and the binocular approach to its therapy. *Vision Research* 114:4–16.
47. Olmos A, Kingdom FA (2004) A biologically inspired algorithm for the recovery of shading and reflectance images. *Perception* 33(12):1463–1473.
48. Pati YC, Rezaiifar R, Krishnaprasad P (1993) Orthogonal matching pursuit: Recursive function approximation with applications to wavelet decomposition in *Signals, Systems and Computers, 1993. 1993 Conference Record of The Twenty-Seventh Asilomar Conference on*. (IEEE), pp. 40–44.
49. Bhatnagar S, Sutton R, Ghavamzadeh M, Lee M (2009) Natural actor-critic algorithms. *Automatica* 45(11).